Available online at www.sciencedirect.com

ScienceDirect

Energy Procedia 00 (2014) 1–10

Energy Procedia

www.elsevier.com/locate/procedia

7th Trondheim CCS Conference, TCCS-7, June 5–6 2013, Trondheim, Norway

CO_2 pipeline integrity: Comparison of a coupled fluid-structure model and uncoupled two-curve methods

E. Aursand[a], C. Dørum[b], M. Hammer[a], A. Morin[a], S.T. Munkejord[a,*], H.O. Nordhagen[b]

[a] *SINTEF Energy Research, P.O. Box 4671 Sluppen, NO-7465 Trondheim, Norway*
[b] *SINTEF Materials and Chemistry, P.O. Box 4670 Sluppen, NO-7465 Trondheim, Norway*

Abstract

One challenge in CCS is related to the prevention of running-ductile fracture in CO_2-carrying pipelines. Commonly used tools for ensuring crack arrest in pipelines hinge mainly on semi-empirical models, which may not be appropriate for CO_2 transport since they have been developed and fitted for natural gas and older pipeline materials, and due to an assumed decoupling of the fluid decompression and fracture propagation phenomena. In this paper, we apply a coupled fluid-structure model to a case with pure dense liquid CO_2 in a modern high-toughness steel pipeline, and compare the results one would obtain from directly applying the uncoupled models to the same case without any re-fitting to test data. For this case, the coupled model indicates that a significantly thicker pipeline wall may be required to prevent running-ductile fracture than what is predicted by the uncoupled models. Therefore, using the uncoupled models for such cases might not be conservative.

Keywords: CO_2 transport, CFD, FEM, fluid-structure, pipeline integrity, running-ductile fracture

1. Introduction

CO_2 capture and storage (CCS) is considered to be an important and necessary means of reducing the world's emission of greenhouse gases. In the International Energy Agency's two-degree scenario (2DS), CCS will account for a CO_2-emission reduction of about 7 Gt per year in 2050 [1]. For the construction of future CCS pipelines, thorough considerations will be needed regarding health, safety and environment (HSE), including pipeline integrity. Furthermore, for economic reasons, it is desirable to reduce oversizing and the use of expensive material qualities. A running-ductile fracture in a high-pressure transport pipeline could be initiated by e.g. corrosion or third-party damage. If this happens, an important question is whether and after how long time the fracture will arrest by itself (self-arrest), or if the fracture will keep running indefinitely.

To answer the question whether a fracture will propagate or not, requires solving a coupled fluid-structure problem [2]. The initial depressurization due to the leak or fracture will cause fluid flow out

*Corresponding author.
Email address: svend.t.munkejord@sintef.no (S.T. Munkejord)

of the pipe, as well as two depressurization waves propagating in opposite directions from the tips of the opening fracture. The pressure waves move relative to the pipeline at a speed equal to the difference between the local speed of sound and the local fluid speed. This couples to the fracture propagation speed, as this speed is mainly controlled by pressure distribution on the opening pipe. Thus, the crack-arrest question boils down to deciding which one of the two propagates the fastest. If the decompression wave is faster than the propagating fracture, the pressure at the fracture will decrease, and the fracture will eventually arrest. If the running fracture is faster than the decompression speed, the pressure distribution at the fracture will be sufficiently high to drive the fracture, and the fracture will not self-arrest.

The most commonly used models for this crack-arrest problem are semi-empirical uncoupled models, such as in the Battelle method [3] and the HLP approach [4]. These models are based on theoretical analysis and full-scale crack-arrest experiments. In the standard codes for gas transmission pipelines (see [5]) the requirements for crack arrest are estimated by the use of these models. They all rely on the fundamental assumption that the decompression wave speed may be uncoupled from the fracture velocity. The commonly employed uncoupled models were developed for pipeline material qualities used 30–40 years ago for transport of natural gas, and worked well in those cases. Due the economical benefits of transporting gas at higher pressures and volumes, the trend seen today is to use pipelines with higher strength and toughness, as well as lower pipe-wall thicknesses. The high toughness of these steels yields a different relationship between the fracture toughness and the fracture velocity, and hence an under-estimate of the fracture velocity as measured in full scale burst tests [6]. There are strong indications that the empirical basis developed earlier (Battelle and HLP) does not apply to these new conditions in the case of CO_2 transport [6].

As mentioned in the review by Aursand *et al.* [7], there are several research challenges when it comes to the fluid- and thermodynamical modelling of transient flow of CO-rich mixtures in pipelines. Of particular relevance for the present study is the fact that even small quantities of some impurities can significantly alter the thermophysical properties of the fluid, including the phase envelopes. The presence of impurities will also affect the wave-propagation velocities of the model [8]. Further, for two-phase and multiphase flow, the speed of sound is not only a thermodynamic state function, but it is also a function of the flow topology. These quantities will affect the depressurization of the pipe and hence the crack-propagation behaviour.

In [9, 10], we presented a fully coupled fluid-structure model for the assessment of running-ductile fracture. Herein, the fluid flow was modelled as one-dimensional inside the pipe and through the crack opening. The ideal-gas equation of state (EOS) was employed for the fluid. The pipe was modelled using the finite-element method with shell elements and a local ductile fracture criterion. The model was validated using data from full-scale tests with steel pipes pressurized with hydrogen and with methane. Good agreement was found between model predictions and experiments, both regarding the pressure and the crack position as a function of time. In [11], the model was augmented with the Span–Wagner reference EOS [12], and the formation of solid CO_2 was accounted for. Experimental data were not available for comparison, but the calculations indicated that a pipeline may be more susceptible to running-ductile fracture when filled with CO_2 than when filled with natural gas.

In this work, the goal is to examine the differences between the predictions of the fully coupled model and the traditional uncoupled models. This is done by defining a single case with parameters in a realistic range, and using the pipeline wall thickness as the design variable which must be chosen such as to prevent running-ductile fracture. The models are compared in terms of *arrestability*, which is defined here as the fracture propagation length for a given pipeline thickness. This is similar to the arrestability criterion proposed in [13], only with pipeline thickness as the design variable instead of steel toughness. The most crucial number found is the *arrest threshold thickness*, which is the thickness at the threshold between fracture arrest (finite fracture length), and running fracture (infinite fracture length).

The uncoupled and coupled models will be presented in Sec. 2 and 3, respectively. The selected test case for the comparison is then defined in Sec. 4, before the results are presented and discussed in Sec. 5. Finally, conclusions are drawn in Sec. 6.

Table 1: Quantities in (1) and (2) which depend on the model used.

	Battelle	HLP (original)	HLP (Sumitomo)
α	C	α_0	$\alpha_0 \left(\frac{Dt}{D_0 t_0}\right)^{\frac{1}{4}}$
β	1/6	β_0	$\beta_0 \left(\frac{D}{D_0}\right)^{\frac{5}{2}} \left(\frac{t}{t_0}\right)^{-\frac{1}{2}}$
γ	1	1	$3.42 \cdot \left[3.22 + 0.20 \left(\frac{t/D}{t_0/D_0}\right)^3\right]^{-1}$
R_f	CVP/A	D_p/A_p	D_p/A_p

2. Uncoupled two-curve models

Methods such as that of Battelle [3] and HLP [4] rely on the fundamental assumption that the decompression wave speed may be uncoupled from the fracture velocity. This means that the decompression wave speed is calculated for an ideal decompression event (full-bore opening in pipe) without the presence of a running fracture. The fracture speed is calculated as a simple function of the pressure at the fracture tip, the pipe geometry and properties of the pipe material used. No interaction between the pipe material and the fluid is taken into account. The above considerations are often turned into decompression speed versus pressure curves (hence *two-curve methods*), where it is said that the fracture will self-arrest if the fracture speed is lower than the decompression speed for all pressures.

2.1. Fracture-velocity models

In the 1970s, the Battelle Memorial Institute proposed such an uncoupled model [3, 14], based on the Charpy test as a toughness measure. This model was elaborated by the High Strength Line Pipe (HLP) Committee [4, 15], and again extended with more parameters in the form of *the Sumitomo version* [13]. These models appear in a variety of forms in the literature, due to differing systems of units and various merging of variables and constants. Though it might not appear so at first sight, all the above uncoupled models may in fact be unified to the same form, where the fracture velocity is given by

$$v_f(p) = \alpha \frac{\bar{\sigma}}{\sqrt{R_f}} \left(\frac{p}{p_a} - 1\right)^{\beta}, \tag{1}$$

with the arrest pressure given by

$$p_a = \gamma \cdot \frac{2t\bar{\sigma}}{3.33\pi R} \arccos\left[\exp\left(-\frac{\pi R_f E}{24\bar{\sigma}^2\sqrt{Rt}}\right)\right]. \tag{2}$$

Here $\bar{\sigma}$ (Pa) is the material flow stress, R_f (J/m^2) is the fracture toughness per fracture area, t (m) is the pipeline wall thickness, R (m) is the outer pipeline radius and E (Pa) is the material elastic modulus. The quantities α (m^2 /kg$^{0.5}$), β (−), γ (−) and R_f (J/m^2) are quantities which depend on the specific model, as indicated in Tab. 1.

As seen, there are two different measures of material toughness used: CVP/A (J/m^2) is the full-size upper-shelf Charpy V-notch energy per fracture area, and D_p/A_p (J/m^2) is the pre-cracked thickness Drop Weight Tear Test (DWTT) energy per area. The constant β_0 is always equal to 0.393, while the quantities C and α_0 supposedly only depend on the amount of backfill (none, soil, water) above the pipeline. Even in the case of no backfill, it is implied that the pipeline is below ground level in a ditch. To our knowledge, no parameters have been fitted to experiments with pipelines on flat ground. Here, tests are performed assuming no backfill, in which case $C = 0.379 \times 10^{-3}$ m^2 kg$^{-0.5}$ [14]. To our knowledge, no reference to α_0 for no backfill has been found in the literature. From [3] we have that C is 38% higher in conditions without backfill than when backfill (0.76 m) is present. We choose to apply the same scaling when going to conditions without backfill for α_0, and get $\alpha_0 = 0.925 \times 10^{-3}$ m^2 kg$^{-0.5}$. The reference geometry for the fitting of α and β is $D_0 = 1219.2$ mm and $t_0 = 18.3$ mm, with $D = 2R$ being the outer pipeline diameter.

Note that the forms of Eqs. (1) and (2), as well as the numerical value of constants, occur in several versions in the literature. These differences stem from corrections for using inconsistent units, as well as from lumping quantities such as the toughness test specimen area, A, and the elastic modulus, E, into constants. The versions here are adapted for use with standard SI units, while revealing as many variables as possible.

2.2. Gas decompression model

The model for gas decompression speed in both uncoupled approaches is derived by considering a pipeline with a stationary fluid at a given initial pressure, and which is suddenly opened at one end. The opening is completely stationary, as opposed to being a running fracture. By assuming one-dimensional and isentropic flow, one may analyse the characteristics of the Euler equations to show that along a rarefaction wave, the fluid velocity depends on the pressure as

$$\frac{\mathrm{d}|u|}{\mathrm{d}p} = -\frac{1}{\rho a}, \tag{3}$$

where ρ is the local density, and a is the local speed of sound. This is called the *real fluid isentropic decompression model*, and shows that the absolute value of the fluid velocity is larger the further down one is on the pressure curve, *i.e.* the closer one is to the opening. Note that this is valid for any fluid, and the behaviour of a specific real fluid is introduced by how the equation of state specifies the pressure dependence of ρ and a, given the isentropic assumption. Since a pressure wave moves at the local speed of sound relative to the fluid, and the initial fluid velocity is zero, the speed of a pressure level relative to the pipeline is given by

$$\begin{aligned} v(p) &= a(p) - |u(p)| \\ &= a(p) - \int_p^{p_i} \frac{1}{\rho(p')a(p')}\mathrm{d}p'. \end{aligned} \tag{4}$$

With an equation of state to find ρ and a, (4) may be used to draw the decompression-speed curve in two-curve methods. It should be noted that the above approach, when used for multiphase flow, assumes no slip between the phases.

2.3. Arrest length

If one has an equation for the fracture velocity given a fluid pressure at the fracture tip, $v_f(p)$, and an equation for finding which fluid pressure level has a given decompression speed, $p_{\mathrm{decomp}}(v)$, one may derive an ordinary differential equation (ODE) for the fracture tip position, L. The function $v_f(p)$ is given by fracture-velocity models such as (1). The function $p_{\mathrm{decomp}}(v)$ is found from the decompression model in Eq. (3), by interpolating an obtained $v(p)$ curve.

The derivative of L with respect to the time, τ, is equal to the fracture velocity, $v_f(p)$, by definition. To evaluate the latter at a given time, τ, one needs the fluid pressure at the fracture tip position, L, at that time. Under the assumptions that the decompression process is unaffected by the presence of the running fracture, and that the decompression starts at the point $L = 0$ at the time $\tau = 0$, this pressure is simply given by the fluid pressure level which moves at a velocity L/τ in the decompression model. The ODE resulting from these assumptions is

$$\frac{\mathrm{d}L}{\mathrm{d}\tau} = v_f = v_f(p_{\mathrm{tip}}(L,\tau)) = v_f(p_{\mathrm{decomp}}(L/\tau)), \tag{5}$$

which may be integrated numerically until arrest is reached, giving a final arrest length, L_a. To obtain a solution, initial conditions are also needed. The approach used with the HLP model [15, 13], which will also be used here, is to set L_0 equal to the pipeline diameter, and set $\tau_0 = L_0/v_i$, where v_i is the decompression speed of the initial pressure level.

3. The coupled model

3.1. Structure model

The pipeline structure has been modelled using the finite-element (FE) code LS-DYNA [16]. With an explicit time-integration scheme, the deformation and fracture of the pipe has been calculated using shell elements and an elasto-plastic constitutive equation [10] with a local ductile fracture criterion [17]. Although pipeline materials often show a certain degree of plastic anisotropy and strain-rate sensitivity, we have for simplicity assumed an isotropic yield criterion (von Mises), with a strain-rate independent non-linear isotropic work-hardening rule.

3.1.1. The isotropic elasto-plastic constitutive equations

The yield function, f, which defines the elastic domain in stress space, is expressed in the form

$$f(\boldsymbol{\sigma}, \epsilon_e) = \sigma_e(\boldsymbol{\sigma}) - (\sigma_0 + R(\epsilon_e)) \tag{6}$$

where $\boldsymbol{\sigma}$ is the stress tensor, σ_e is the von Mises equivalent stress, ϵ_e is the corresponding equivalent plastic strain, and σ_0 is the yield stress in the reference equation. The isotropic strain-rate-independent work-hardening rule is defined as

$$R = \sigma_0 + Q_1(1 - \exp(-C_1\epsilon_e)) + Q_2(1 - \exp(-C_2\epsilon_e)) \tag{7}$$

where Q_i and C_i are the quasi-static work-hardening parameters. After the onset of necking in an uni-axial tension test, an imposed hydrostatic tension will form in the neck, and the uni-axial stress state must be corrected. This correction is done using an FE analysis, where C_i and Q_i are adjusted such that the experimental and simulated engineering stress-strain curves match. The work-hardening parameters in (7) were calibrated from tensile tests on smooth axisymmetric specimens oriented in the circumferential direction (reference direction) of the pipe. Quasi-static tests were done in room temperature and at an average strain-rate of $10^{-3}\,\mathrm{s}^{-1}$. The force and minimum cross-section area of the specimen were continuously measured until fracture. The parameters identified for the quasi-static work-hardening rule are given in Tab. 3.

3.1.2. The fracture model

From the perspective of material modelling, the greatest obstacle to simulate a running-ductile fracture is the lack of a complete understanding of the physical mechanisms governing the phenomenon (see *e.g.* [18]). The fracture typically has velocity in the pipe axial direction of about 100 to 300 $\mathrm{m{\cdot}s^{-1}}$, and typically propagates as a slant fracture. However, in the literature, there are indications that the exact mechanisms leading to the slant fracture are not necessary to capture in order to achieve a good engineering representation and prediction of the fracture resistance [19]. In this paper, a simplified approach to describe fracture is used. The fracture model assumes that damage evolution (e.g. void growth) does not influence the material behaviour. That is, there is no material softening of the material prior to fracture. Fracture propagation is described by element erosion when the Cockcroft-Latham (CL) ductile fracture criterion [17] is fulfilled in one integration point. The CL fracture criterion states that fracture occurs when the tensile principal stress integrated over the strain path reaches a critical value

$$W = \int_0^{\epsilon_e} \langle\sigma_I\rangle \mathrm{d}\epsilon_e \leq W_c,\ \langle\sigma_I\rangle = \max(\sigma_I, 0) \tag{8}$$

Here σ_I is the major principal stress and W_c is a material constant that should be determined from a suitable experiment. In this work, W_c has been calibrated from uniaxial tests (described earlier) at quasi-static loading conditions, where the value of W_c was found by integrating the true stress-plastic strain curve up to point of failure. Results show $W_c = 1095\,\mathrm{MPa}$ (see Tab. 3).

3.2. Fluid model

The one-dimensional compressible flow of pure CO_2 is modelled using the homogeneous equilibrium model and the Span–Wagner [12] reference equation of state (EOS). The flow model, with source terms accounting for the effects of leakage through the fracture, are

$$\begin{aligned} \frac{\partial \rho}{\partial \tau} + \frac{\partial (\rho u)}{\partial x} &= -\zeta \\ \frac{\partial (\rho u)}{\partial \tau} + \frac{\partial \left(\rho u^2\right)}{\partial x} &= -u\zeta \\ \frac{\partial E}{\partial \tau} + \frac{\partial \left([E+p]\, u\right)}{\partial x} &= -\left(\frac{E_e + p_e}{\rho_e}\right)\zeta, \end{aligned} \tag{9}$$

where x is the axial position, τ is the time, p is the pressure, ρ is the density, and u is the velocity in the x-direction. Subscripts e indicate the corresponding quantities at the point of escape/outflow. The quantity E is the total energy per volume, given by

$$E = \rho\left(e + \frac{1}{2}u^2\right), \tag{10}$$

where e is the fluid internal energy per mass.

For each set of local (ρ, E) obtained from the flow equations (9), a density–energy flash routine [20] using the Span–Wagner EOS is used to find the corresponding local equilibrium state. All three possible phases are covered, as the Span–Wagner EOS of state was extended to the solid state (dry ice) using an empirical polynomial for $\rho_s(T)$ [21]. For single-phase flow, the above formulation (9) amounts to the Euler equations. The formulation is also applicable to multiphase flow if one assumes that there is no velocity difference (slip) between the phases. For such flows, the model is often referred to as the homogeneous equilibrium model. The relationships between the variables of the homogeneous equilibrium model (9) and the properties of the individual phases are

$$\begin{aligned} u &= u_g = u_l = u_s \\ \rho &= \alpha_g\rho_g + \alpha_l\rho_l + \alpha_s\rho_s \\ E &= \alpha_g\rho_g\left(e_g + u^2/2\right) + \alpha_l\rho_l\left(e_l + u^2/2\right) + \alpha_s\rho_s\left(e_s + u^2/2\right). \end{aligned} \tag{11}$$

The quantity ζ in (9) should represent the rate of mass loss through the fracture, per volume of pipe. In view of the fluid model, the fracture is characterized by a function $r_e(x)$, indicating half of the fracture width at the given point (see Fig. 1a). If one considers a cell of length dx, the mass flux through the fracture at this point is $\rho_e u_e$, giving a total mass-loss rate of $\rho_e u_e 2 r_e \mathrm{d}x$. Since the volume of this cell is $A\mathrm{d}x$, where A is the cross-sectional area of the pipe, the rate of mass loss per volume of pipe at any point is given by

$$\zeta = \rho_e u_e \frac{2r_e}{A}. \tag{12}$$

The modelling of the source terms are described in [11]. The governing equations (9) are solved numerically with the finite-volume method, using a single-stage two-cell MUSTA [22, 23] scheme for the spatial derivatives, and forward Euler for time integration. The time-step is limited by a Courant–Friedrichs–Lewy (CFL) condition for compressible flow, with a CFL-number of 0.5.

3.3. Coupling

The coupled model performs the following scheme (see Fig. 1b) at each time step:

1. The structure model communicates the current fracture profile $r_e(x)$ to the fluid model.
2. The fluid model uses this fracture profile to integrate the fluid state to the current time.
3. The pressure profile for the current time is communicated back to the structure model.

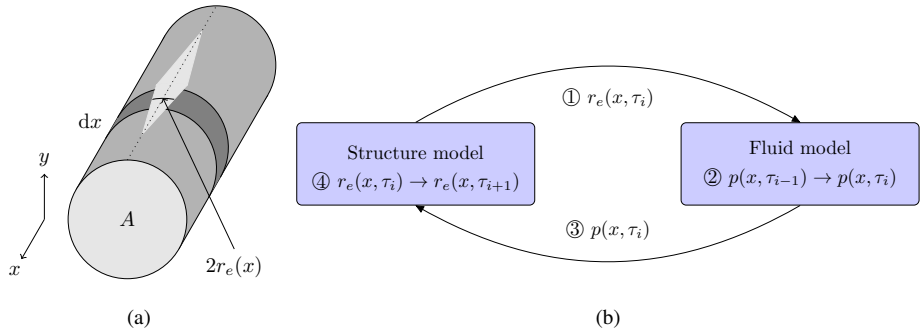

(a) (b)

Figure 1: a) Illustration of the pipeline as seen by the fluid model, defining the quantities A and $r_e(x)$ in (12). b) Flow-chart illustrating the coupling between the structural model and the fluid model.

Table 2: The initial conditions of the pipeline, where D is the pipeline diameter, P_i is the initial fluid pressure, T_i is the initial fluid temperature, u_i is the initial fluid velocity, and L_i is the initial fracture length (from the centre).

D (m)	P_i (Pa)	T_i (K)	u_i (m·s^{-1})	L_i (m)	$r_{e,i}$ (m)
0.559	1.0×10^7	300	0	0.559	5×10^{-3}

4. The structure model uses the pressure profile at the current time to apply a load to its structural elements, and integrates the pipe-material state one time step ahead.

In the cases run here the time-step length required by the structure model is smaller than the one required by the fluid model. This means that stage 2 in the above scheme only involves a single time-step in the fluid model, smaller than what is required by the CFL criterion. Specifically for the present cases, the structure model requires a time-step length of about 10^{-6} s, while the fluid model requires about 10^{-5} s.

4. Test case

4.1. Pipeline initial conditions

The initial conditions of the pipeline and its contents are shown in Tab. 2. In both coupled and uncoupled models, the initial crack is $L_0 = D$ long from the centre. In the coupled model, the initial crack also has a width, given by $r_{e,i}$. In the uncoupled models, the initial crack length is only relevant when tracking the crack-tip position in time (Sec. 2.3), and not when doing simple two-curve considerations. The fluid is initialized as stationary ($u_i = 0$), at pressure P_i and temperature T_i.

4.2. Material parameters

Specimens for the material calibration was taken from an API 5L-X65 TMR steel pipeline, with outer diameter 559 mm and wall thickness 13.5 mm. The pipeline had previously been exposed to a full-scale crack-arrest experiment with hydrogen gas [24]. The parameters used to represent this material in the models are shown in Tab. 3. The parameters $\sigma_{0,\mathrm{FEM}}$, C_i and Q_i have been adjusted to fit the finite-element model to an experimental stress-plastic strain curve. This is the reason why $\sigma_{0,\mathrm{FEM}}$ is different from $\sigma_{0,(0.2\%\mathrm{offset})}$, which is used when calculating $\bar{\sigma}$ in the uncoupled models. The average plastic flow stress of the material, $\bar{\sigma}$, must be interpreted as an average flow stress acting in the plastic zone ahead of a crack tip, and cannot be precisely defined [25]. Different definitions are used in the uncoupled approaches. For Battelle, $\bar{\sigma} = \sigma_{0,(0.2\%\mathrm{offset})} + 68.95\,\mathrm{MPa} = 574.95\,\mathrm{MPa}$, and for HLP $\bar{\sigma} = 0.5(\sigma_{0,(0.2\%\mathrm{offset})} + \sigma_{\mathrm{TS}}) = 544.5\,\mathrm{MPa}$, with $\sigma_{0,(0.2\%\mathrm{offset})} = 506\,\mathrm{MPa}$ and $\sigma_{\mathrm{TS}} = 583.0\,\mathrm{MPa}$.

Table 3: Pipeline steel parameters for the uncoupled models (top), and the finite-element model used in the coupled approach (bottom).

	$\bar{\sigma}$ (Pa)	$\frac{\mathrm{CVP}}{A}$ (J/m^2)	$\frac{D_p}{A_p}$ (J/m^2)	E (Pa)
Battelle	5.750×10^8	5.84×10^6	–	2.06×10^{11}
HLP	5.445×10^8	–	5.68×10^6	2.06×10^{11}

	$\sigma_{0,\mathrm{FEM}}$ (Pa)	Q_1 (Pa)	Q_2 (Pa)	C_1 (−)	C_2 (−)	W_c (Pa)
FEM	4.540×10^8	3.986×10^8	1.766×10^8	0.9745	19.765	10.95×10^8

4.3. Coupled model domain and boundary conditions

Due to the symmetry of the case, the simulation was performed in a domain starting from the centre of the initial fracture ($x = 0$), until $x = 10\,\mathrm{m}$. Symmetry boundary conditions were set at $x = 0$, while at the opposite end, a transparent boundary condition was used for the fluid in order to prevent pressure wave reflection. A convergence test on the fluid model showed that 100 cells per metre gave reasonable accuracy, and this cell density in the axial direction was used in both the fluid model and the structure model, giving 1000 cells or shell elements in axial direction in total. The structural model had 70 elements in the circumferential direction. Regarding the grid employed for the structural model, it was chosen based on experience. However, no convergence test was performed, since numerical simulations of fracture is well known to be inherently dependent on the grid resolution used.

The coupled model will simulate a pipeline on flat ground, since the inclusion of the dynamic effects of a surrounding ditch of gravel and soil requires further work.

5. Results and discussion

Arrestability was evaluated with the case described in Sec. 4 using the pipeline thickness t as the variable. With the three variants of the uncoupled model described in Sec. 2, the arrest threshold thickness was first found by the two-curve method, *i.e.* by decreasing t gradually until reaching the point of first contact between the fracture-velocity curve and the decompression curve. The fracture-velocity curves were generated as described in Sec. 2.1, while the decompression curve was generated from (4) using the Span–Wagner EOS for CO_2. Two-curve plots for all three models, at the arrest threshold, can be seen in Fig. 3. The arrest threshold thicknesses are summarized in Tab. 4. In order to examine the transition, the method described in Sec. 2.3 was used to plot the arrest length L_a as a function of pipeline thickness in Fig. 2. The arrest length is the final fracture length from the centre of the fracture, including the initial length.

The coupled model described in Sec. 3 was run with the same case, while varying the pipeline thickness until the arrest threshold was found. The threshold is displayed in Tab. 4, while the arrest length is plotted as a function of pipeline thickness in Fig. 4. When comparing the coupled model with the uncoupled models in this way, two differences become apparent: First, while the uncoupled models generally agree on the arrest threshold thickness within $\approx 1\,\mathrm{mm}$, the coupled model indicates that more than double the thickness is required to prevent a running-ductile fracture. Second, the transition from immediate arrest to running fracture happens over a range of approximately 0.5 mm in the coupled model, as compared to 0.15 mm or less with the uncoupled models.

The most important of these differences is clearly the first, which shows a large difference in the required pipeline thickness. We see three main reasons for the large difference in arrest threshold thickness. First, the coupled model describes the actual process in a more physically complete way. Second, the uncoupled models have not been adapted to CO_2 pipelines. Third, some of the assumptions in the coupled model may be on the conservative side. An example of the latter is the fact that the internal pipeline pressure from the fluid code at an axial position is used to apply a load on all structural elements at that position, while in reality the pressure is expected to decrease as one moves closer to the opening. This approximation is likely to overestimate the force on the opening flanks. Nevertheless, good agreement with both the experimentally obainted final crack-propagation lengths and pressure time histories at the crack position (12 o'clock) was

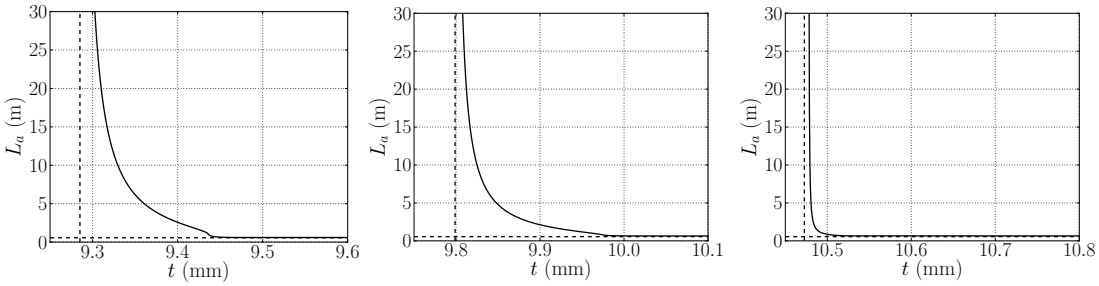

Figure 2: The arrest length as a function of pipeline thickness calculated using the uncoupled models a) Battelle, b) HLP (original) and c) HLP (Sumitomo). The horizontal dashed line indicates the initial fracture length, and the vertical one indicates the arrest threshold.

Table 4: Arrest threshold thickness found with the various methods

Battelle	HLP (original)	HLP (Sumitomo)	Coupled
9.29 mm	9.80 mm	10.47 mm	≈ 24.7 mm

obtained in [10]. Additionally, the coupled model simulates a pipeline on flat ground, while the uncoupled models are fitted to experiments with pipelines in a ditch. Using no ditch is a conservative approximation, as ditches are likely to damp the outward speed of the flanks which helps drive the fracture. Finally, the use of shell elements with a thickness larger than the in-plane dimensions, which is the case at the arrest threshold thickness found here, will tend to underestimate the fracture resistance. However, upon their time of fracture, the fractured elements had a thickness smaller than the in-plane dimensions, so that this thickness effect might not be of great significance.

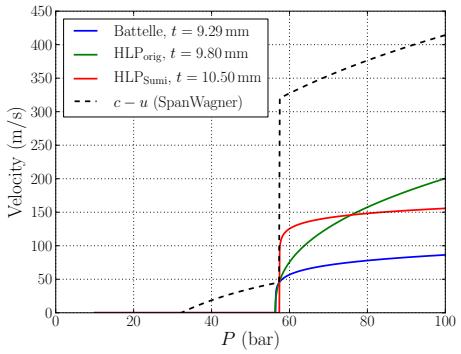

Figure 3: Two-curve plots of the three uncoupled models, each at the corresponding arrest threshold thickness. Solid lines are fracture-velocity curves, while the dashed line is the decompression curve.

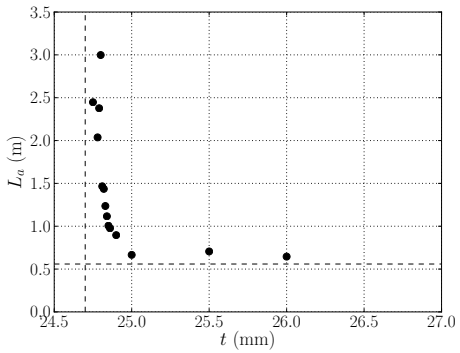

Figure 4: The arrest length as a function of pipeline thickness calculated using the coupled model. The horizontal dashed line indicates the initial fracture length, and the vertical dashed line indicates the arrest threshold thickness.

6. Conclusion

In this work, three semi-empirical uncoupled models (Battelle, HLP and the Sumitomo version of HLP) for running-ductile fracture assessment have been compared to a fully coupled fluid-structure model for the case of a pipeline filled with CO_2. For a given pipeline material and geometry, the minimum pipeline wall thickness was found at which a running-ductile fracture would arrest. This threshold thickness predicted by the fully coupled model was more than twice as large as that given by the uncoupled models. This is an

indication that the threshold thickness given by the uncoupled models is underpredicted. However, some of the assumptions in the coupled model are conservative. The differing results of the present study underline the need for high-quality experiments to allow for further model development and validation.

Acknowledgements

This publication has been produced with support from the BIGCCS Centre, performed under the Norwegian research program Centres for Environment-friendly Energy Research (FME). The authors acknowledge the following partners for their contributions: Aker Solutions, ConocoPhillips, Gassco, Shell, Statoil, TOTAL, GDF SUEZ and the Research Council of Norway (193816/S60).

References

[1] IEA, Energy Technology Perspectives, 2012.
[2] H. Mahgerefteh, O. Atti, Modeling low-temperature–induced failure of pressurized pipelines, AIChE J. 52 (3) (2006) 1248–1256. doi:10.1002/aic.10719.
[3] W. A. Maxey, Fracture initiation, propagation and arrest, in: Fifth Symposium on Line Pipe Research, American Gas Association, Houston, Texas, USA, 1974, pp. J1–J31.
[4] E. Sugie, M. Matsuoka, H. Akiyama, T. Mimura, Y. Kawaguchi, A study of shear crack-propagation in gas-pressurized pipelines, J. Press. Vess. – T. ASME 104 (4) (1982) 338–343.
[5] G. Mannucci, G. Demofonti, Control of ductile facture propagation in X 80 gas linepipe, J. Pipeline Eng. 10 (3) (2011) 133–145.
[6] B. N. Leis, X.-K. Zhu, T. P. Forte, E. B. Clark, Modeling running fracture in pipelines – Past, present, and plausible future directions, in: 11th International Conference on Fracture, ICF11, Vol. 8, 2005, pp. 5759–5764.
[7] P. Aursand, M. Hammer, S. T. Munkejord, Ø. Wilhelmsen, Pipeline transport of CO_2 mixtures: Models for transient simulation, Int. J. Greenh. Gas Con. 15 (2013) 174–185. doi:10.1016/j.ijggc.2013.02.012.
[8] S. T. Munkejord, J. P. Jakobsen, A. Austegard, M. J. Mølnvik, Thermo- and fluid-dynamical modelling of two-phase multi-component carbon dioxide mixtures, Int. J. Greenh. Gas Con. 4 (4) (2010) 589–596. doi:10.1016/j.ijggc.2010.02.003.
[9] T. Berstad, C. Dørum, J. P. Jakobsen, S. Kragset, H. Li, H. Lund, A. Morin, S. T. Munkejord, M. J. Mølnvik, H. O. Nordhagen, E. Østby, CO_2 pipeline integrity: A new evaluation methodology, Energy Procedia 4 (2011) 3000–3007. doi:10.1016/j.egypro.2011.02.210.
[10] H. O. Nordhagen, S. Kragset, T. Berstad, A. Morin, C. Dørum, S. T. Munkejord, A new coupled fluid-structure modelling methodology for running ductile fracture, Comput. Struct. 94–95 (2012) 13–21. doi:10.1016/j.compstruc.2012.01.004.
[11] E. Aursand, P. Aursand, T. Berstad, C. Dørum, M. Hammer, S. T. Munkejord, H. O. Nordhagen, CO_2 pipeline integrity: A coupled fluid-structure model using a reference equation of state for CO_2, Energy Procedia 37 (2013) 3113–3122. doi:10.1016/j.egypro.2013.06.197.
[12] R. Span, W. Wagner, A new equation of state for carbon dioxide covering the fluid region from the triple-point temperature to 1100 K at pressures up to 800 MPa, J. Phys. Chem. Ref. Data 25 (6) (1996) 1509–1596. doi:10.1063/1.555991.
[13] R. Higuchi, H. Makino, I. Takeuchi, New concept and test method on running ductile fracture arrest for high pressure gas pipeline, in: 24th World Gas Conference, WGC 2009, Vol. 4, International Gas Union, Buenos Aires, Argentina, 2009, pp. 2730–2737.
[14] D. Rudland, G. Wilkowski, B. Rothwell, The effects of soil properties on the fracture speeds of propagating axial cracks in line pipe steels, in: 6th Biennial International Pipeline Conference, IPC, Vol. 3 PART A, ASME, Calgary, Canada, 2006, pp. 73–82.
[15] H. Makino, T. Inoue, S. Endo, T. Kubo, T. Matsumoto, Simulation method for shear fracture propagation in natural gas transmission pipelines, Int. J. Offshore Polar Eng. 14 (1) (2004) 60–68.
[16] J. O. Hallquist, LS-DYNA Keyword User's Manual, Livermore Software Technology Corporation (2007).
[17] M. G. Cockcroft, D. J. Latham, Ductility and the workability of metals, J. Inst. Metals 96 (1968) 33–39.
[18] J. Besson, Continuum models of ductile fracture: A review, Int. J. Damage Mech. 19 (1) (2009) 3–52. doi:10.1177/1056789509103482.
[19] K. L. Nielsen, J. W. Hutchinson, Cohesive traction-separation laws for tearing of ductile metal plates, Int. J. Impact Eng. 48 (SI) (2011) 15–23. doi:10.1016/j.ijimpeng.2011.02.009.
[20] K. E. T. Giljarhus, S. T. Munkejord, G. Skaugen, Solution of the Span-Wagner equation of state using a density-energy state function for fluid-dynamic simulation of carbon dioxide, Ind. Eng. Chem. Res. 51 (2) (2012) 1006–1014. doi:10.1021/ie201748a.
[21] M. Hammer, Å. Ervik, S. T. Munkejord, Method using a density-energy state function with a reference equation of state for fluid-dynamics simulation of vapor-liquid-solid carbon dioxide, Ind. Eng. Chem. Res. 52 (29) (2013) 9965–9978. doi:10.1021/ie303516m.
[22] E. F. Toro, MUSTA: A multi-stage numerical flux, Appl. Numer. Math. 56 (10-11) (2006) 1464 – 1479.
[23] S. T. Munkejord, S. Evje, T. Flåtten, The multi-stage centred-scheme approach applied to a drift-flux two-phase flow model, Int. J. Numer. Meth. Fl. 52 (6) (2006) 679–705.
[24] S. Aihara, H. I. Lange, K. Misawa, Y. Imai, Y. Sedei, E. Østby, C. Thaulow, Full scale burst test of hydrogen gas X65 pipeline, in: 8th International Pipeline Conference, IPC 2010, ASME, Calgary, Alberta, Canada, 2010, pp. 415–422.
[25] G. T. Hahn, M. Sarrate, A. R. Rosenfield, Criteria for crack extension in cylindrical pressure vessels, Int. J. Fracture 5 (3) (1969) 187–210.